STRUCTURAL DYNAMIC INVESTIGATION OF ADAPTIVE WING DEMONSTRATOR WITHIN SADE PROJECT

Gennady A. Amiryants[1], Vladimir P. Kulesh[1], Victor A. Malyutin[1], Andrey V. Smotrov[1], Alexander V. Chedrik[1]

[1] Central aerohydrodynamic institute (TsAGI)
stataer@tsagi.ru

Keywords: adaptive wing, aeroelastic analysis, videogrammetry.

Abstract: Main task of the SADE (SmArt High Lift DEvices for Next Generation Wing) project was investigation of the next generation "smart" high lift devices directed for lift-to-drag ratio, fuel efficiency increase as also noise, emission decrease at all flight regimes, especially at take-off/landing regimes.

Some concepts of adaptive control were investigated in this project. Significant step in the investigation of the most perspective ones was manufacturing and testing of large-scaled demonstrator in TsAGI big size low-speed T-101 wind tunnel.

In this paper mainly the results of flutter and divergence theoretical-experimental investigations, results of ground vibration tests – GVT, as well as the results of "smart" leading edge elastic deformations optical measurements are presented.

To measure the deformations of "smart" leading edge upper and lower surfaces noncontact videogrammetric method and double-channel measuring system were developed. Digital cameras were located inside of the left endplate above and under the wing. Additional controller based on compact computer in the left endplate was used for distance image transfer in the image acquisition system on the base of PC.

1 INTRODUCTION

Modern airplanes need to adapt their wings in flight for different requirements such as safe, high lift performance during take-off/landing and efficient cruise flight. Up-to-date high lift systems consist of movable control surfaces which increase high lift performance in their extended position. One of the basic problems in such concept is the laminarisation technology of such devices that leads to increase aerodynamic quality (lift to drag ratio) and fuel efficiency of transport airplanes, while reducing noise and emissions in all flight regimes (take-off and landing cases in the first instance). It is the aim of the SADE project of the 7th European Framework Programme that investigates and develops slotless high lift devices appropriate for next generation wings.

One of the variants of such devices, developed by German specialists (DLR and EADS [1-6]) is Smart Leading Edge (SLE) device with direct attachment to the wing box, as illustrated on Figure 1. The slotless attachment to the wingbox and the adaptability of required shape for the droop function is enabled by continuous and selectively elastic structures with integrated actuators.

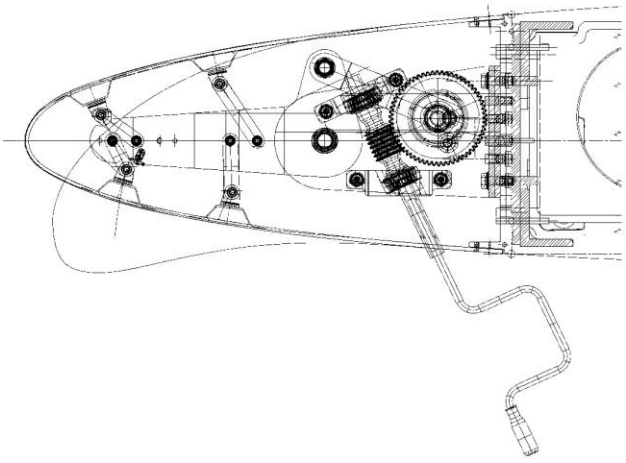

Figure 1: Smart leading edge – SLE of SADE demonstrator (Design and manufacturing of DLR and EADS)

Along with other partners, on the base of other concepts of adaptive structures, for example [7, 8], TsAGI took participation in design [9-11], fabrication, stiffness and ground vibration tests of the next generation wing compartment model with smart controls. TsAGI provided also this demonstrator wind tunnel T-101 tests. Last stage of the work fulfilled by TsAGI with European partners participation was pressure distribution, balance and strain-gage measurements, optical videogrammetric measurements, safe wind tunnel tests taking into account flutter and other aeroelasticity problems. CAD geometry and finite element model were created for the flutter and eigenvalue analyses to insure safety of the wind tunnel measurements.

2 THE WING DEMONSTRATOR

The demonstrator represents a straight wing of 5 m span and 3 m chord mounted on T-101 remote-rotate base. It was installed in the work section horizontally on the upper structure of the wind tunnel and was limited by end-plates. Wing box includes two metal spars and connected with them upper and lower milled metal panels. The CAD geometry configuration of the wind tunnel demonstrator with supporting elements and side plates is shown on Figure 2.

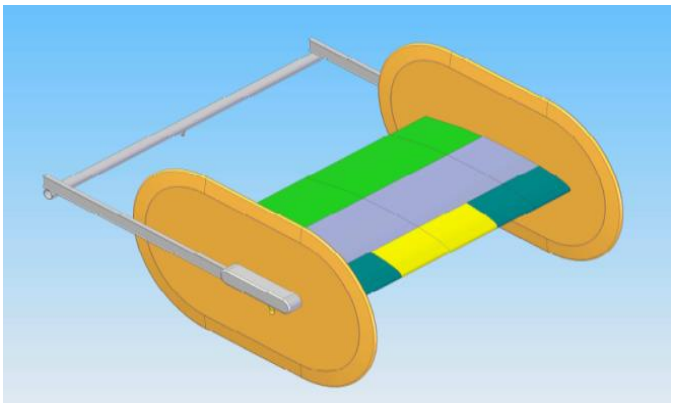

Figure 2: CAD geometry of the wing demonstrator

Three sections of the smart leading edge were attached to the front spar. Each section included flexible composite skin that was deflected by drive mechanisms during wing-tunnel tests. The skin of the smart leading edge was fabricated using glass fiber reinforced plastic. Single-section flap was mounted on rear spar. Deflecting angle of the flap is set up by virtue of rigid replaceable coupling plates.

Setup of demonstrator in test-section of wind tunnel T-101 is shown on Figure 3.

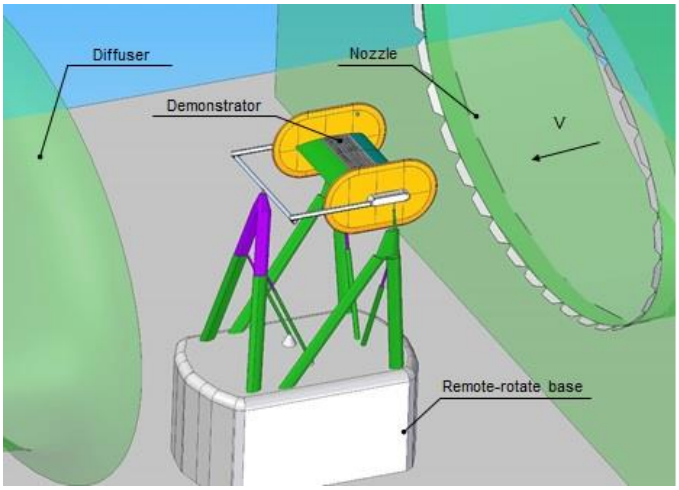

Figure 3: Setup of demonstrator in working section of wind tunnel T-101

3 FINITE ELEMENT MODEL OF THE WING DEMONSTRATOR

In order to perform flutter and eigenvalue analysis of the demonstrator a complete finite element model (FEM) shown on Figure 4 was created. The wing model was attached to the upper structure of wind tunnel balance at three struts. In the model the attachment points were hinged joints, visible as red markers.

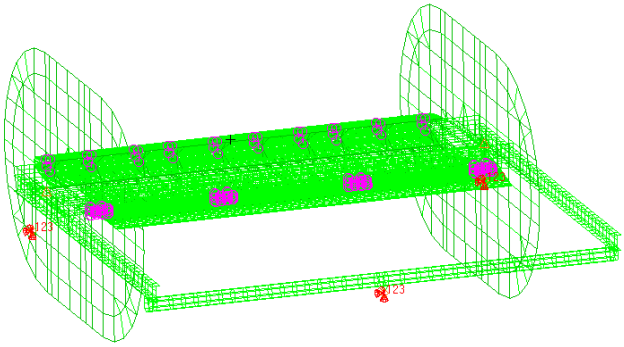

Figure 4: Finite element model with boundary conditions

Extend mechanism of leading edge consisted of some worm drives connected with flexible skin - four drives in middle part and three drives in each outer part. In FEM it was realized by virtue of MPC and RBE2 elements shown on Figure 5.

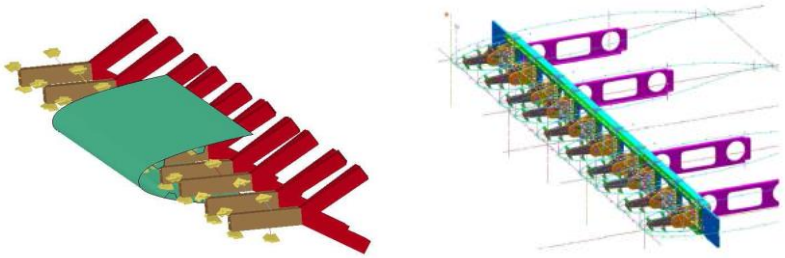

Fig. 5. Active leading edge mechanism CAD and corresponding FE-model

The trailing edge flap was connected to the wing structure via MPC elements, displayed in magenta colors, on Figure 4. The total number of elements used in the finite element model is 6642, number of nodes is 4675.

4 EIGENVALUE AND FLUTTER ANALYSIS

Calculation-experimental investigations of aeroelasticity characteristics of demonstrator were done before wind tunnel tests. A total of 20 eigenvalues were calculated and used for the flutter analysis. Comparison between vibration test results and corresponding results of calculations for the first 11 modes are presented in Table 1.

Mode number	1	2	3	4	5	6	7	8	9	10	11
Analysis frequency , Hz	3.58	8.299	9.38	14.47	15.71	13.25	13.9	14.9	18.28	21.6	24.5
Experimental frequency, Hz	3.86	8.297	9.125	-	16.72	12.22	13.37	13.76	17	-	-
Damping coefficient ζ, %	4.18	0.55	0.86	-	0.41	1.18	0.63	0.66	0.45	-	-
Difference, %	7.2	-0.02	-2.7	-	6.4	-8.4	-3.9	-8.2	-7.5	-	-

Table 1: Comparison between vibration test and corresponding calculations for the first 11 modes

The first wing mode is shown on Figure 6.

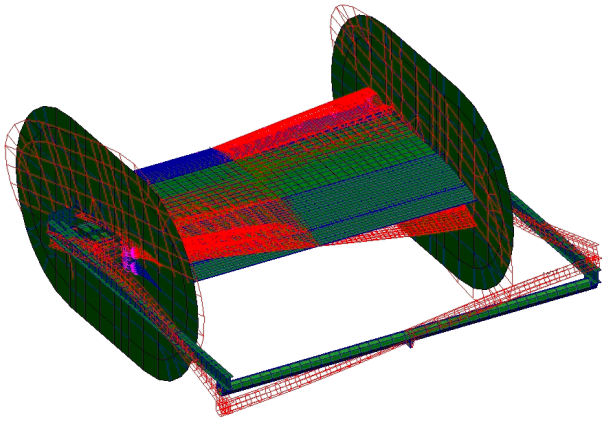

Figure 6: The first mode of SADE-project demonstrator vibrations

The general coupled fluid-structure equations are non-linear. This non-linearity comes not only from the flow equations but also from large displacements and material non-linearities. In the present analysis the airspeed is in the low sub-sonic range and hence incompressible potential flow, using doublet-lattice panel method, will provide a fairly good approximation of the aerodynamics. The linearized FE equations of motion $\mathbf{v}(t) = \tilde{\mathbf{v}} \cdot e^{i\omega t}$, may be written as,

$$\mathbf{M}\ddot{\mathbf{v}} + \mathbf{K}\mathbf{v} - q\mathbf{A}(k)\mathbf{v} = 0, \tag{1}$$

where **M** and **K** are the structural FE mass and stiffness matrices respectively. The aerodynamic part may be defined in terms of the dynamic pressure, $q = \rho \cdot u^2 / 2$, a complex non-symmetric aerodynamic influence coefficient matrix **A** and the reduced frequency $k = \omega \cdot b / u$, where ρ is the air-density, ω is the angular frequency, u is the airspeed and b is the semi-cord length. Equation (1) may be defined as a non-linear eigenvalue problem, due to the **A** matrix dependence on the reduced frequency k

$$\left[\left(\mathbf{M} + \frac{\rho}{2}\left(\frac{b}{k}\right)^2 \mathbf{A}(k)\right) - \lambda\mathbf{K}\right]\tilde{\mathbf{v}} = 0\,, \tag{2}$$

where the complex aeroelastic eigenvalue is defined as $\lambda = 1/\omega^2$. And iterative solution methodology is thus needed in order to find the complex eigenvalues. In order to reduce the size of the problem it is standard practice to use approximate modal solution techniques, based on the solution the elastic eigenvalue problem. The corresponding aeroelastic eigenvalue problem using a modal base $\mathbf{\Psi}$ is defined as

$$\left[\left(\mathbf{I} + \frac{\rho}{2}\left(\frac{b}{k}\right)^2 \mathbf{\Psi}^{\mathrm{T}}\mathbf{A}(k)\mathbf{\Psi}\right) - \lambda\mathbf{\Omega}\right]\tilde{\mathbf{v}} = 0\,, \tag{3}$$

where the two diagonal modal matrixes $\mathbf{I} = \mathbf{\Psi}^{\mathrm{T}}\mathbf{M}\mathbf{\Psi}$ and $\mathbf{\Omega} = \mathbf{\Psi}^{\mathrm{T}}\mathbf{K}\mathbf{\Psi}$, $m = 1,\ldots \mathrm{M}$, corresponding to the mass-normalized modal masses and the eigenfrequencies. In practice, it is common to rewrite equation (3) in first order form in order to transform the complex eigenvalue problem into a real value problem [12].

The goal of the aeroelastic analysis is to find the critical speed and unstable non-damped flutter behavior of the structure. The p-k method is widely accepted for flutter analysis and used also in the present work. More specifically, the MSC.Nastran ZONA module is used [13].

The aerodynamic panels and coupled finite element nodes used in this flutter analysis are displayed on Figure 7. The speed range considered in analysis is from 0 to 500 m/s.

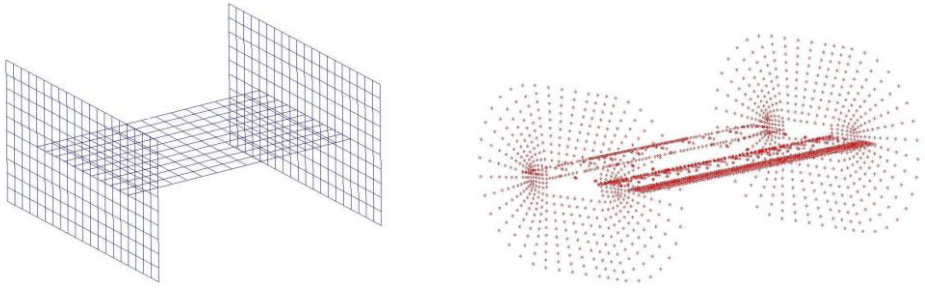

Figure 7: Aerodynamic panels (blue) and corresponding FE coupling nodes (red)

In the present model the worst case with no structural damping was considered.

In the plots, the important parameter to track is when the damping curve is passing the zero damping level. Definition of flutter used here is when the damping becomes positive. The result from the Mach 0.2 (68 m/s) simulation, plotted on Figure 8, shows that mode 3 and 4 are critical at approximately 285 m/s. So the critical speed is outside the operational range (up to 50 m/s).

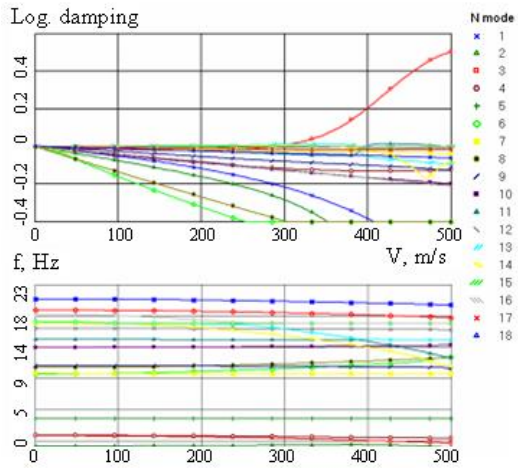

Figure 8: Results of SADE-project demonstrator flutter calculations.

5 GROUND VIBRATION TESTS OF DEMONSTRATOR

GVT handlings, acquisition and express-processing of the data were fulfilled mainly by A.Smotrov and S.Smotrova [14] using program-device system based on Laser Scanning Vibrometer (LSV) Polytec PSV-400H4. The main modules of LSV are controller OFV-5000 and high-performance sensor-based scanning head PSV-I-400 that provides with automatic focusing and focus storage.

Scanning head PSV-I-400 used for data storage was cabled with controlling and processing device located in mobile transport container (packer). This made it possible for scanning head fixed on tripod to be located in suitable for measurements place.

Impulse excitation of free damped vibrations was implemented by means of impact force-measuring hammer PCB 086E80 that was connected to PSV-E-400. Excitation points on the demonstrator were chosen on metallic parts of structure at stiffening ribs.

The measurements of the demonstrator vibrations were carried out on the distance from 5 to 10 m. Noncontact information read-out were performed from 3 different viewpoints (front, left side, rear).

GVT results such as mode frequencies, damping constants and mode shapes were demonstrated graphically. The first experimental mode of wing demonstrator is shown on Figure 9.

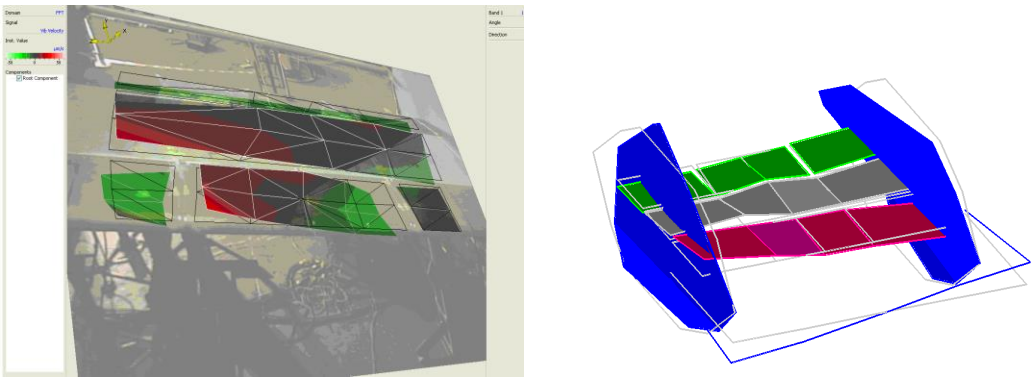

Figure 9: The first experimental mode of wing demonstrator

6 WIND TUNNEL TESTS

Main aims of the wind tunnel tests were: pressure distribution measurements for three wing cross-sections, balance measurements, measurements of smart leading edge skin deformations, measurements of SLE structural strain under aerodynamic loading.

For example, comparison between wind tunnel pressure distribution measurements (TsAGI) and 3D CFD (DLR and FOI), Figure 10, and pressure distribution measurements for three wing cross-sections, landing configuration, Figure 11, are presented.

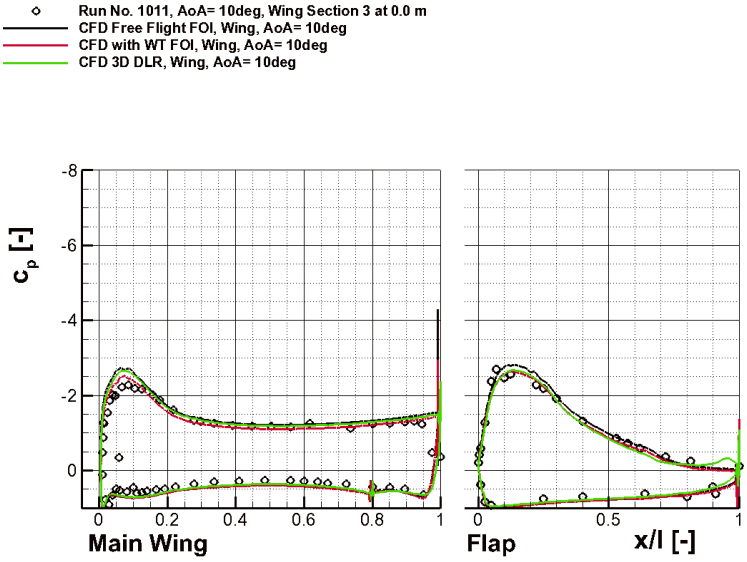

Figure 10: Comparison between wind tunnel pressure distribution measurements) and 3D CFD – for angle of attack AoA=10°, 50 m/s

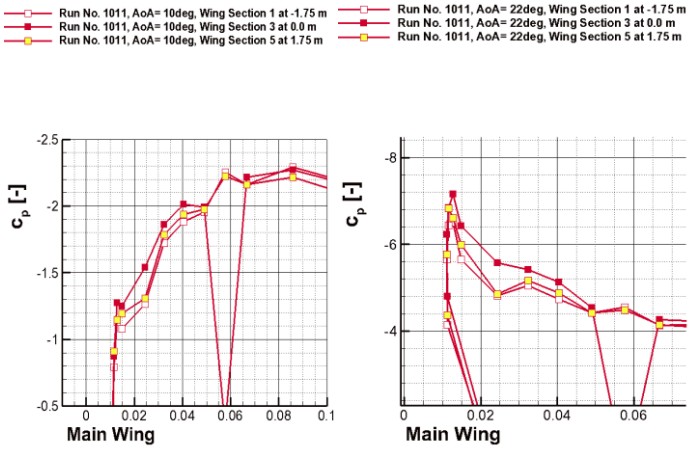

Figure 11: Pressure distribution measurements for three wing cross-sections, landing configuration, 50 m/s at AoA=10° and 22°

Main attention dedicated here to the measurements of smart leading edge skin deformations.

6.1 Videogrammetry method of deformation measuring

The method of digital videogrammetry as effective method for non-contact measurements of geometric shape parameters and deformation of a model in wind tunnel flow was developed and used. This method has replaced the traditional method of photogrammetry since the beginning of the 90s [15, 16]. The essence of the method is following: one can find

3 spatial coordinates *x*, *y*, *z* of the point of the object knowing only its 2 response coordinates *u*,*v* in the digital image. Indisputable advantages of this method are non-contact, simultaneous measurement in a large number of points and high spatial resolution provided him wide application in scientific research, including experimental aerodynamics [15-18].

Implementation of the method involves placing of a special optical system in a wind tunnel or a test bench, which is usually fixed and rigidly connected to the coordinate system of a tunnel or a bench. However, there is a problem regarding measurement of deformation of large-scale models in large wind tunnels and in field conditions. The optical system in this case can not be considered as stationary. Furthermore, area of measurement of large-scale model usually can not be covered by a single optical system – it is required two or more channel measuring system.

The aim of this work was to develop and apply the videogrammetry method for measuring deformation of large-scale wing model in a wind tunnel T-101. Achieving this goal is related to the following tasks:

– creation of a special multi-channel optical system, providing simultaneous registration of two or more coherent images of different parts of the model surface;

– development of methods and means of mutual linking (group calibration) of several videogrammetry channels;

– development of methods of linking of coordinate systems of different in general case mutually movable cameras with the coordinate system of the model.

6.2 Test object and experimental facility

The scheme of experimental facility is shown on Figure 13, and wing-demonstrator scheme - on Figure 12.

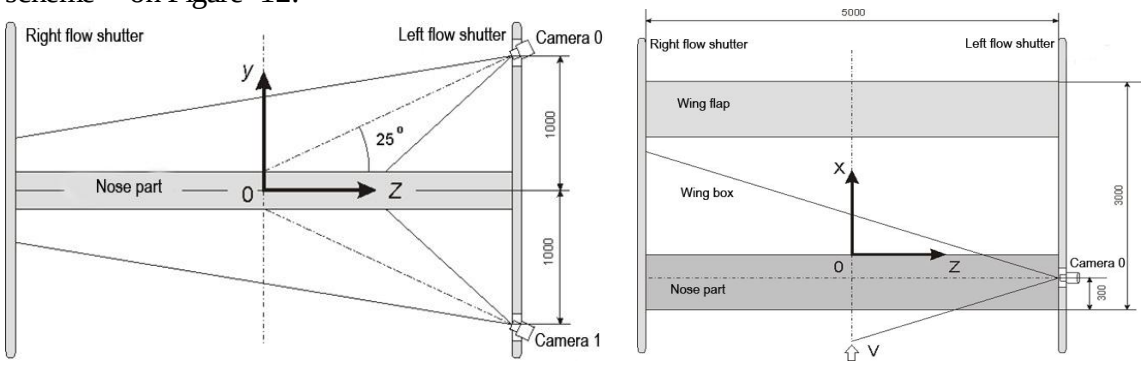

a) front view b) top view

Figure 12: Overall layout of demonstrator and cameras placement (cameras shown not in scale)

For simultaneous measurements of upper and lower wing surface deformation (fulfilled with participation of K. Kopoteva) a two-channel videogrammetry system was developed. The system used two digital cameras, placed on the left end-plate of demonstrator (Figure 14a). Cameras with a resolution of 1392x1040 pixels were equipped with lenses having a focal length of 16 mm. Images transfer from both cameras was carried out via Ethernet.

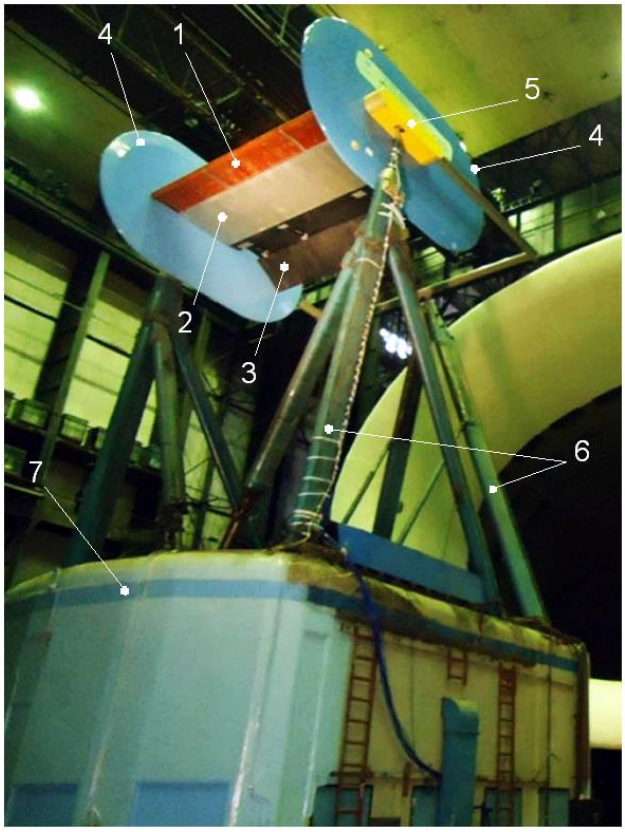

Figure 13: Experimental facility in working section of wind tunnel T-101 (1 – SLE, 2 – wing box, 3 – wing flap, 4 – end-plate, 5 – fairing, 6 and 7 – upper structure of the mechanical balance)

The origin of coordinate system *O* was placed at the point of wing chord on the front part of wing box in vertical plane of symmetry of the model. *Ox* axis is directed along the chord downstream, *Oy* axis – upwards, perpendicular to the chord, and *Oz* axis – along the span in the direction of the cameras. Three interconnected systems of markers were placed on the surface of the model: two measuring for each of the channels and one supporting that is observed by both cameras (Figure 14b).

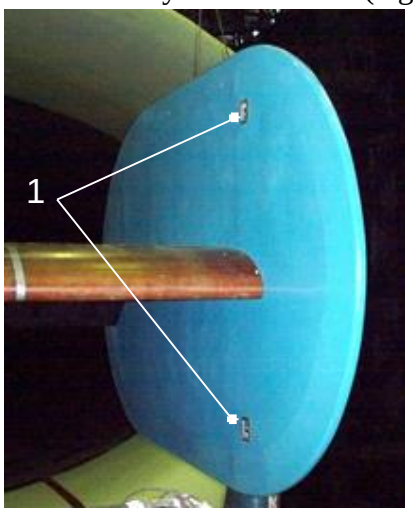

a) left end-plate

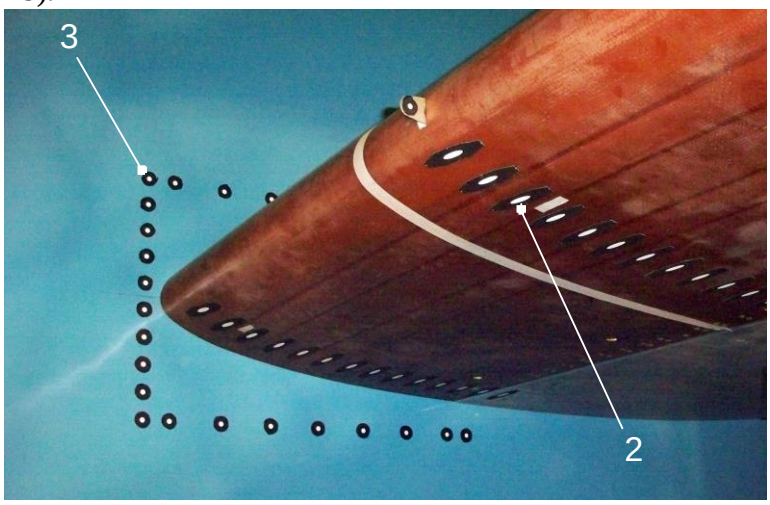

b) right end-plate

Figure14: Location of the cameras and marker system (1 – location of the cameras, 2 – measuring markers, 3 – supporting markers)

Measuring systems of markers were placed on the top and bottom surfaces of the nose part within ten sections with values of *z*-coordinate 1300, 1050, 950, 475, 0, 475, 950, 1050, 1600 and 2480 mm. Each section contained 14 markers. The first marker was located on the wing box at point x = 25 mm and following ones – along the profile arc to the tip of SLE with 50 mm step. Markers had an elliptical shape. Their sizes (along small axis from 3 mm to 9 mm) and orientation were determined so that markers in the images would have the form of circle with a diameter about 5 pixels. The support system of markers included two lines of markers: first line consisted of markers that were already on the top and bottom of the wing box at points with *x*-coordinate 25 mm, and another one included a group of additional markers placed on the surface of opposite (right) end-plate visible by the two cameras. Coordinates of all markers were measured with manual measuring tool with the highest precision.

Regular lighting system of the test section of the wind tunnel served as a source of continuous illumination for the wing surface.

6.3 Operating characteristics and the coordinate system

The essence of the videogrammetry method is the following: one can find 3 spatial coordinates x, y, z of the point of the object knowing only its 2 response coordinates u, v in the digital image. To resolve the uncertainty problem of finding the unknown spatial coordinates x, y, z of a point, prior information about known *z*-coordinate of the markers on the model was used [18, 19]. Operating characteristics of the measuring system can be written as a system of two nonlinear equations:

$$\begin{aligned} x &= (z - z_0)\frac{M_{11}(u-u_0) + M_{12}(v-v_0) + M_{13}w_0}{M_{31}(u-u_0) + M_{32}(v-v_0) + M_{33}w_0} + x_0 \\ y &= (z - z_0)\frac{M_{21}(u-u_0) + M_{22}(v-v_0) + M_{23}w_0}{M_{31}(u-u_0) + M_{32}(v-v_0) + M_{33}w_0} + y_0 \end{aligned}, \tag{4}$$

where:

u_0,v_0 – coordinates of the center of the image, i.e. the cross point of objective lens optic axis and digital camera matrix plane (in pixels);

w_0 – rear section of the receiver objective (in pixels);

x_0,y_0,z_0– coordinates of the center of the receiving lens (projection center) in the coordinate system of the model (in metric units);

M_{ij} – elements of rotation matrix, directional cosines. Rotation matrix elements are functions of the orientation angles α, β, γ of camera coordinates in the coordinate system of the object.

Lens distortion was taken into account by corrections:

$$\begin{aligned} u &\approx u_0 + (u' - u_0)\cdot(1-\delta), \\ v &\approx v_0 + (v' - v_0)\cdot(1-\delta). \end{aligned} \tag{5}$$

where $\delta = \dfrac{d}{w_0^2}\left[(u-u_0)^2 + (v-v_0)^2\right]$, d – the ratio of distortion.

Parameters u_0, v_0, w_0 and d are called as parameters interior orientation, and x_0,y_0,z_0 and α, β, γ – parameters of exterior orientation.

The determination of numerical values of operation characteristics coefficients (4) was implemented in two stages:

– The first stage involved the definition of the interior orientation parameters for each camera with customized objective using certified reference tool in laboratory environment. This stage allowed estimating the instrumental measurement error by two coordinates by the value of ±0.2 mm.

– The second stage included the definition of the current values of exterior orientation parameters of the operation characteristics for each registered frame by the group of reference markers located on the wing box and opposite (right) end-plate. This made it possible to exclude the influence of uncontrolled shifts of cameras resulting from general deformation of the model.

6.4 Measuring process and data handling

Measuring of deformation of wing model was performed on SLE in a deflected position (takeoff and landing) and undeflected position (cruising regime). In each case, the measurements of x, y coordinates for all the markers on the angles of attack of -10, -5, 0, 5, 10, 15, 19 and 22 degrees were carried out. Measurements of coordinates of "undeformed" model markers were preliminary fulfilled for all angles of attack without flow in the wind tunnel and then they were performed at the same angles at flow rates of 30, 40 and 50 m/s.

Images processing was performed using a set of standard and special programs. While processing the following steps were performed: measurement of u, v coordinates of marker projection centers on each image; calculation of x, y coordinates of corresponding points on the surface, according to the formulas of the operation characteristic (4, 5); finding deformation parameters by subtracting the coordinates of points on the surface in a "non-flow" state from the coordinates in the current "with flow" state.

6.5 Measuring process and data handling

The results of measurements of SLE profile shape in deflected and undeflected states without flow are shown in the plots (Figure 15).

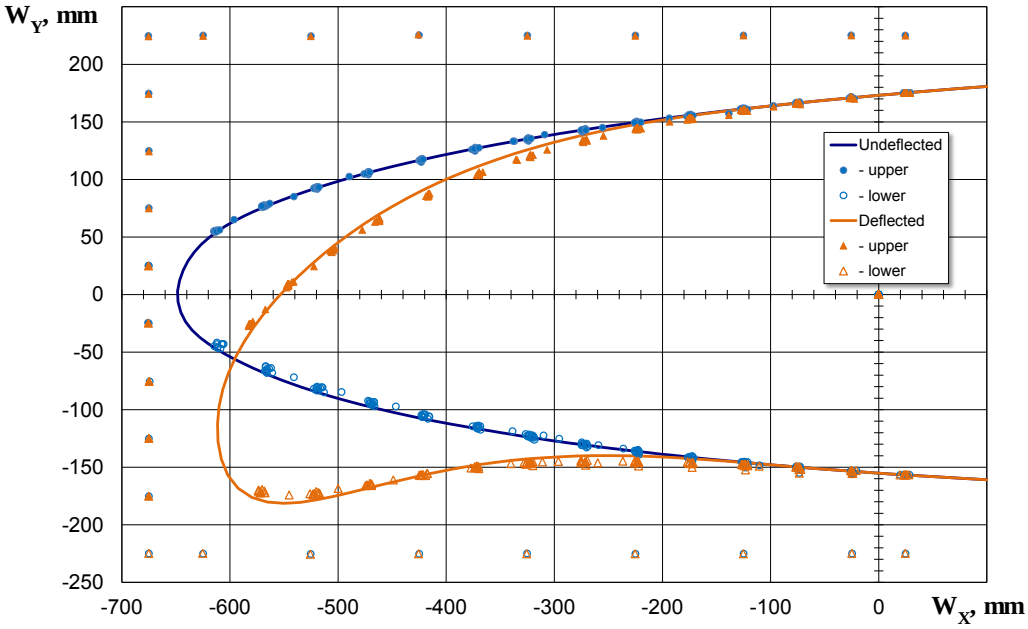

Figure 15: The results of measurements of SLE shape in deflected and undeflected states

Results of measurements of surface deformation, defined as the deviation Δx_0 and Δy_0 of corresponding coordinates in "with flow" state from "undeformed" "non-flow" state at each angle of attack, are presented in the form of two-dimensional matrices on a rectangular grid with the purpose of three-dimensional imaging capability of deformation fields. Shown on Figure 16 is an example of such visualization of the deflection fields along the axis Oy of upper and lower surfaces in the most deformed state in the test mode with the undeflected SLE at angle of attack of 22° and flow speed of 50 m/s.

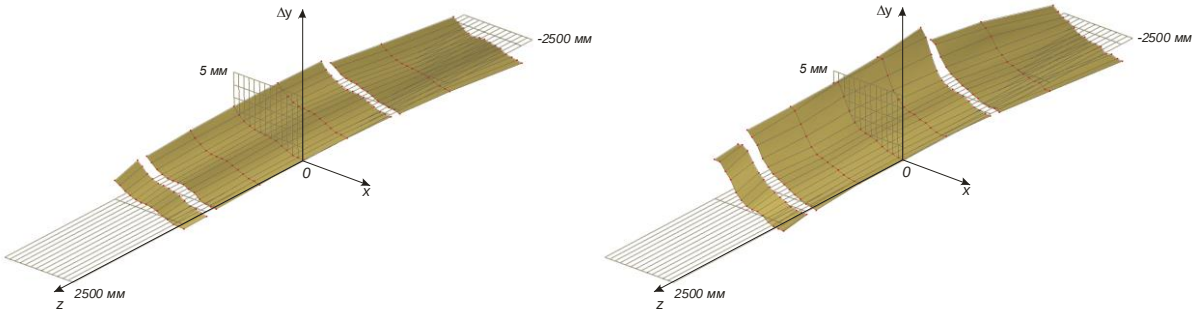

(a) (b)

Figure 16: Three-dimensional presentation of deformation fields of top (a) and bottom (b) sections of SLE surfaces

The maximum deviation along Oy axis was up to 5 mm in the leading area on the bottom surface of the middle section of the SLE. Longitudinal wavy variations of vertical deviations of the surface, which correlate with the configuration of structure supporting the skin, were observed in all test regimes. Formation of ledges at the adjacent section joints of wing leading edge part reaching maximum values of 1 mm on the lower surface on the right joint and 1.5 mm on the left one was also seen.

7 CONCLUSIONS

Detailed FE model of the SADE project demonstrator was created for the preliminary (before wind tunnel tests) eigenvalue and flutter analysis. Verification of FE model by virtue of ground vibration test was performed.

A classical flutter investigation was performed on the FEM of the demonstrator structure at wind tunnel tests conditions. The result showed that flutter for the finite element model is absent in the speed range to be tested in wind tunnel.

Main aims of the TsAGI T-101 wind tunnel tests of the large-scale demonstrator were: pressure distribution measurements for three wing cross-sections, strain-stress measurements of smart leading edge structure elements, balance measurements and measurements of smart leading edge skin deformations under aerodynamic loading.

Videogrammetry method and two-channel measuring system for measuring deformation of large-scale models in wind tunnels were developed.

Location scheme of digital cameras on the model was tested. Algorithms of dynamic linking for model coordinate system that allows preventing the influence of displacement of cameras due to global model deformation were developed.

Practically important research results of deformation of adaptive SLE of the SADE project demonstrator wing model were obtained.

8 ACKNOWLEDGMENTS

This research was performed as a part of the international project SADE of 7th European Framework Programme.

9 REFERENCES

[1] H.P. Monner, J. Riemenschneider, Background and recent results of the European project ‘Smart High Lift Devices for Next Generation Wings’, 1st EASN Association Workshop on Aerostructures, 7-8 Oct 2010, Paris, France aerodynamics. - Sensors and Systems, 2004. № 3. -pp. 22-27.

[2] H. P. Monner, J. Riemenschneider, Morphing high lift structures: Smart leading edge device and smart single slotted flap, Aerodays 2011, 30th March - 1st April 2011, Madrid, Spain

[3] M. Kintscher, 5 Years research on Smart Droop Nose devices at DLR-FA - a retrospective, Wissenschaftstag FA, DLR, 18.October 2012, Braunschweig, Deutschland.

[4] M. Kintscher, O. Heintze, H. P. Monner, "Structural Design of a Smart Leading Edge Device for Seamless and Gapless High Lift Systems", 1st EASN Association Workshop on Aerostructures, 7-8 Oct 2010, Paris, France

[5] T. Kühn, "Aerodynamic Optimization of a Two-Dimensional Two-Element High Lift Airfoil with a Smart Droop Nose Device", 1st EASN Association Workshop on Aerostructures, 7-8 Oct 2010, Paris, France

[6] J. Kirn, T. Lorkowski, H. Baier, "Development of Flexible Matrix Composites (FMC) for Fluidic Actuators in Morphing Systems", 1st EASN Association Workshop on Aerostructures, 7-8 Oct 2010, Paris, France

[7] S. Ameduri, A. Concilio, E. Daniele, A droop nose laboratory demonstrator: Experimental characterization and validation, ICAS 2012: 23rd International Conference on Adaptive Structures and Technologies, October 11-13, 2012, Nanjing, China

[8] G. A. A. Thuwis, M.M. Abdalla, Z. Gürdal, A Variable Stiffness Skin for Morphing High-lift Devices, 1st EASN Association Workshop on Aerostructures, 7-8 Oct 2010, Paris, France

[9] Amiryants G. Adaptive Selectively Deformable Structures. Proceedings of 21-th ICAS Congress, Melbourne, 1998.

[10] Amiryants G.A., Grigoriev V.D., Kawiecki G. Selectively Deformable Structures Analysis. International Forum on Aeroelasticity and Structural Dynamics, Amsterdam, 2003.

[11] G.A.Amiryants, V.A.Malyutin, V.P.Timohin, F.Z.Ishmuratov, Selectively Deformable Structures for Design of Adaptive Wings "Smart" Elements, 1st EASN Association Workshop on Aerostructures, 7-8 Oct 2010, Paris, France

[12] Wright, J. R. and Cooper, J. E., Introduction to Aircraft Aeroelasticity and Loads, John Wiley &Sons, Ltd, 2007.

[13] MSC.Nastran Version 68, Aeroelastic Analysis, User's Guide, 2002.

[14] A. Smotrov, S. Smotrova, Amiryants G.A., Chedrik A.V., Rapid Ground Vibration Test of Complex-shaped Construction by Laser Scanning Vibrometer, International Meeting on Optical Measurement Techniques and Industrial Applications, 20-21 Nov. 2013, Rijswijk, The Netherlands

[15] Kulesh V.P., Fonov S.D. Measurement of parameters of motion and deformation of aircraft model in a wind tunnel by videogrammetry method. // scientific notes of TsAGI, 1998. v.XXIX, №1-2. – pp.165-176.

[16] Lobanov A.N. Photogrammetry. – Nedra. 1984. - 552 p.

[17] Burner A.W., Tianshu Liu. Videogrammetric model deformation measurement technique. // J. of Aircr., 38. 4, pp. 745-754, 2001.

[18] Kulesh V.P. Non-contact measurement of geometrical parameters of shape, motion and deformation of objects in experimental aerodynamics. - Sensors and Systems, № 3. -pp. 22-27, 2004.

[19] Bosnjakov S.M., Kulesh V.P., Fonov S.D. et al. Videogrammetric system for studying of movement and deformation of real-scaled helicopter rotor blades., SPIE – 1999. Vol. 3516, 0277-786X/99, Part One, pp. 196-209.

10 COPYRIGHT STATEMENTS